



AgPO₂F₂ and Ag₉(PO₂F₂)₁₄: the first Ag(I) and Ag(I)/Ag(II) difluorophosphates with complex crystal structures

Journal:	<i>Dalton Transactions</i>
Manuscript ID:	DT-ART-05-2015-002004.R1
Article Type:	Paper
Date Submitted by the Author:	29-Jun-2015
Complete List of Authors:	Malinowski, Przemysław; University of Warsaw, Centre of New Technologies; Albert-Ludwigs-Universität Freiburg, Institut für Anorganische und Analytische Chemie Freiburger Materialforschungszentrum Kurzydłowski, Dominik; University of Warsaw, Centre of New Technologies Grochala, Wojciech; University of Warsaw, Centre of New Technologies

Cite this: DOI: 10.1039/c0xx00000x

www.rsc.org/xxxxxx

ARTICLE TYPE

AgPO₂F₂ and Ag₉(PO₂F₂)₁₄: the first Ag(I) and Ag(I)/Ag(II) difluorophosphates with complex crystal structures

Przemysław J. Malinowski,^{a*} Dominik Kurzydłowski,^{a,b*} and Wojciech Grochala^{a*}

Received (in XXX, XXX) Xth XXXXXXXXXX 20XX, Accepted Xth XXXXXXXXXX 20XX

DOI: 10.1039/b000000x

The reaction of AgF₂ with P₂O₃F₄ yields a mixed valence Ag^I/Ag^{II} difluorophosphate salt with Ag^I₄Ag^{II}₅(PO₂F₂)₁₄ stoichiometry – the first Ag(II)-PO₂F₂ system known. This highly moisture sensitive brown solid is thermally stable up to 120°C, which points at further feasible extension of the chemistry of Ag(II)-PO₂F₂ systems. The crystal structure shows a very complex bonding pattern, comprising of polymeric Ag^{II}₅(PO₂F₂)₁₄⁴⁻ anions and two types of Ag^I cations. One particular Ag^{II} site present in the crystal structure of Ag₉(PO₂F₂)₁₄ is the first known example of square pyramidal penta-coordinated Ag(II) in oxo-ligand environment. Ag(I)PO₂F₂ – the product of the thermal decomposition of Ag₉(PO₂F₂)₁₄ – has also been characterized by the means of thermal analysis, IR spectroscopy and X-ray powder diffraction. It has complicated crystal structure as well, which consists of infinite 1D [Ag^IO_{4/2}] chains which are linked into more complex 3D structures via OPO bridges. The PO₂F₂⁻ anions bind to cations in both compounds as bidentate oxo-ligands. The terminal F atoms tend to point inside the van der Waals cavities in the crystal structure of both compounds. All important structure details for both title compounds were corroborated by the DFT calculations.

Introduction

Divalent silver can be considered as an exotic species among transition metal cations. Its inorganic chemistry is full of peculiarities including extremely high Ag^{II}/Ag^I oxidation potential (the largest among divalent metal cations) reaching +2.90 V in 33% oleum,¹ high degree of covalence of the Ag(II)-F bonds,² unusually strong magnetic coupling in some of its fluorides³ and oxoanionic compounds⁴ as well as atypical pathways of the thermal decomposition of its salts.⁵ Recently it has been postulated that 2D coordination polymers of Ag(II) could potentially exhibit high-temperature superconductivity (HTSC).⁶ However, compounds containing Ag(II) are predominated by fluorides, none of which exhibits strong 2D antiferromagnetic (AFM) coupling – a property that is believed to be a prerequisite to the appearance of HTSC. Therefore extension of Ag(II) chemistry to oxo- ligands constitutes a natural research route. It is noteworthy to point out that among the few known Ag(II)-O systems there are several, such as AgSO₄ or M_n^IAg^{II}(SO₃F)_{n+2} (M = Na, K, Ag, n = 2, 3),^{7,8} which exhibit very strong AFM coupling. The limited number of Ag(II) compounds containing oxoanions results from the fact that only SO₄²⁻ and fluorine-containing anions like SO₃F⁻^{9,10} and SO₃CF₃⁻^{11,12} are capable of withstanding the extremely positive oxidation potential of Ag^{II}.

To date the difluorophosphate anion, PO₂F₂⁻, has been largely omitted in the research on Ag(II) chemistry although available data point at its significant resistance towards oxidation (as exemplified by the existence of Xe(II)-PO₂F₂ salts).¹³ Currently systems containing this anion draw increased attention as they may be used as ionic liquids¹⁴ or battery electrolytes.¹⁵ However, the chemistry of PO₂F₂⁻, particularly its inorganic salts, is underdeveloped with vibrational spectra^{13,16,17,18} reported and only seven crystal structures of its metal salts currently known (K⁺,¹⁹ Rb⁺,²⁰ Cs⁺,²⁰ NH₄⁺²¹, Cu(II)²², Co(II)-2MeCN²² as well as (SbF₄O₂PF₂)₂²³).

In an attempt to extend Ag(II) chemistry towards connections containing the PO₂F₂⁻ anion, and specifically targeting

Ag^{II}(PO₂F₂)₂ (which we failed to obtain), we have managed to prepare two novel compounds: Ag^IPO₂F₂ (1) and Ag₉(PO₂F₂)₁₄ (=Ag^I₄Ag^{II}₅(PO₂F₂)₁₄, (2)). We have characterized their thermal stability and decomposition pathways, vibrational spectra and magnetic properties, as well as their crystal structure (with additional support from DFT calculations). The mixed-valence Ag₉(PO₂F₂)₁₄ constitutes the first example of compound containing Ag^{II} cations coordinated by PO₂F₂⁻, thus proving that this anion is capable of withstanding the oxidizing prowess of Ag^{II}. It is simultaneously the fifth known Ag(I)/Ag(II) mixed-valence compound, others being two complex compounds with organic ligands,^{24,25} Ag^I₂Ag^{II}(SO₃F)₇ and Ag^IAg^{II}(SbF₆)₃.²⁶ The high thermal stability of Ag₉(PO₂F₂)₁₄ – and the novel synthetic pathways described here – open the possibility of further extending the chemistry of Ag^{II} with difluorophosphate ligands.

Experimental section

P₂O₃F₄ was obtained by dehydration of anhydrous HPO₂F₂ with P₂O₅ (99%, Sigma-Aldrich) according to procedure described elsewhere.²⁷ Anhydrous HPO₂F₂ was obtained from commercially available hemihydrate (ABCR, 98%) by dehydrating with P₂O₅ as reported in the literature.²⁸ AgF₂ (98%) and AgF (99%) were purchased from Sigma-Aldrich and CF₃COOAg (purum) from Fluka.

Due to the high reactivity of the compounds used in the study, all manipulations were carried out in dry Ar filled glovebox (MBraun labmaster, O₂ < 20 ppm and H₂O < 4 ppm at peak concentrations) or in a fluoropolymer (FEP and PTFE) vacuum line equipped with a monel vacuum gauge (Ashcroft, T6500). Due to the reactivity of AgF₂ and HF towards glass, all the reaction vessels were made of fluoropolymers (FEP).

The IR spectra were measured with Bruker Vertex 80V vacuum FT-IR spectrometer. The powdered samples were placed on AgCl (MIR) or PE (FIR) windows. Powder XRD patterns were recorded at room temperature on PANalytical X'Pert Pro powder diffractometer equipped with Co K_{α1/2} lamp. The samples were flame sealed in 0.3 or 0.5 mm thick quartz

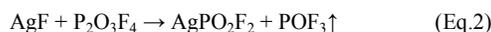
capillaries (Hilgenberg, 0.01 mm wall thickness). The 2Θ step of 0.013° was used. To avoid high absorption of radiation by **2** only a thin film of the powder was spread on the walls of the capillary. TGA/DSC/EGA experiments were performed in Netzsch STA 409PG TGA/DSC furnace coupled with quadrupole mass spectrometer (Aeolos QMS 403C) and argon (6.0) used as a purging gas. The samples were placed in alumina crucibles (4.06 mg of AgPO_2F_2 and 6.00 mg of $\text{Ag}_9(\text{PO}_2\text{F}_2)_{14}$, scan range 30–500°C, heating rate 5 K/min). Magnetic susceptibility measurements were performed in SQUID-VSM magnetometer (Quantum Design) for sample placed in an air-tight FEP/PTFE capsule (8.90 mg, magnetic field 100 Oe, 1.8–300 K, scan rate 1 K/min, ZFC and FC data sets collected). Theoretical calculations were performed with the plane-wave-basis DFT approach with inclusion of Coulomb repulsion (U) for 4d electrons of silver (the DFT+ U method as formulated by Liechtenstein *et al.*²⁹); we used the values of U and J equal to 5 eV and 1 eV, respectively. We utilized the Perdew-Burke-Ernzerhof exchange-correlation functional,³⁰ and the projector-augmented-wave method,³¹ as implemented in the VASP 5.2 code³². The cut-off energy of the plane waves was set to 900 eV with a self-consistent-field convergence criterion of $1 \cdot 10^{-6}$ eV. Valence electrons ($2s$ and $2p$ for P, O and F; $4d$ and $5s$ for Ag) have been treated explicitly, while standard VASP pseudopotentials³³ were used for the description of core electrons. The k -point mesh was generated in such a way that the spacing between the k -points was approximately 0.18 \AA^{-1} . During geometry optimization, the ionic relaxation was continued until the forces acting on individual atoms were less than 0.002 eV/\AA . Visualization of structures has been done with VESTA.³⁴

Synthesis of AgPO_2F_2

Direct reaction between AgF and HPO_2F_2 yielded impure product. This is consistent with previous studies that conclude that the reaction of HPO_2F_2 with fluorides yields contaminated products due to fluorination of the anion.¹³ **1** was found to form efficiently in the displacement reaction between HPO_2F_2 and CF_3COOAg according to equation (1):



Trifluoroacetic acid can be easily removed by pumping off the sample. Another successful synthetic strategy was the reaction of AgF and $\text{P}_2\text{O}_3\text{F}_4$ according to the reaction (2):



Considerable amounts of unreacted AgF present in the sample after 1 hour of the reaction (2) point to its slow kinetics and therefore render it unsuitable for synthesis of larger amounts of pure **1**. Thermal decomposition of **2** at 180°C constitutes the third route towards **1**; it has to be carried out in an open reactor to avoid side reactions of **1** with the evolved POF_3 (see discussion in Thermal analysis section below). The process should also be finished immediately after complete decolorization of the sample to minimize concomitant decomposition of AgPO_2F_2 at that temperature.

Synthesis of $\text{Ag}_9(\text{PO}_2\text{F}_2)_{14}$

2 was obtained in the reaction between AgF_2 (1.14 mmol) and $\text{P}_2\text{O}_3\text{F}_4$ (5.39 mmol) according to formal equation (Eq. 3):



The bracketed dioxygen on the product side of the equation is due to formal balancing of the reaction equation rather than is an

experimentally established finding (*cf.* also thermal behaviour of $\text{Ag}_9(\text{PO}_2\text{F}_2)_{14}$ presented below). After condensing $\text{P}_2\text{O}_3\text{F}_4$ above cold (LN_2 cooled reactor) AgF_2 the reaction mixture was left to warm. Upon contact of the molten anhydride with AgF_2 gas evolution ensued and the liquid turned dark violet. To prevent contact of AgF_2 and the forming product with POF_3 the amount of $\text{P}_2\text{O}_3\text{F}_4$ was sufficient to completely cover the whole solid fraction. To remove POF_3 formed during the reaction the reaction mixture was frozen in -40°C bath and POF_3 was pumped out. Then the reaction was left to proceed at room temperature until no bubbling was noticeable (*i.e.* around 20 minutes). The excessive $\text{P}_2\text{O}_3\text{F}_4$ was then removed under vacuum and 305 mg of a dry dark brown powder was obtained, which corresponds well with the expected mass of **2** (302 mg).

The reaction of AgF_2 and HPO_2F_2 which targeted $\text{Ag}^{\text{II}}(\text{PO}_2\text{F}_2)_2$ yielded very contaminated greyish product, the majority of the crystalline phase being $\text{Ag}^{\text{I}}\text{PO}_2\text{F}_2$ as based on the XRDP of the sample. The subsequent characterization of **2** has been performed using the sample obtained through reaction (3).

Attempt of synthesis of $\text{Ag}(\text{PO}_2\text{F}_2)_2$

POF_3 prepared in the course of the studies was reacted at -40°C with AgF_2 yielding brown solid that turned gray upon warming to room temperature with evolution of large amounts of gases including O_2 as indicated by the O_2 sensor in the glovebox. The identity of the brown phase was not investigated in depth due to its marked instability, but it could correspond to $\text{Ag}^{\text{II}}(\text{OPF}_4)_2$ or to the desired $\text{Ag}^{\text{II}}(\text{PO}_2\text{F}_2)_2$. The conclusion from this study relevant for reaction described by Eq. 3 is that the evolving POF_3 has to be isolated from AgF_2 during synthesis of **2**.

Results and discussion

Crystal structure

Since the compounds could only be obtained as powders, their crystal structure determination was performed using powder X-ray diffraction data. However, due to poor precision in localization of light elements (O, F) restraints were applied both on PO_2F_2^- geometry (*ca.* 1.47 \AA for P-O and 1.51 \AA for P-F, as taken from $\text{Cu}(\text{PO}_2\text{F}_2)_2$ ²²) and on selected Ag-O bonds. Restrictions on a given Ag-O bond were applied only when its length from unrestricted refinement was unreasonably short ($< 2 \text{ \AA}$ for Ag(II) and $< 2.3 \text{ \AA}$ for pentacoordinated Ag(I)) and when the bond valence sum (BVS) for Ag(I) was significantly deviating from unity. Details regarding applied restraints are provided in ESI. Additional support for the crystal structures comes from optimizations performed using DFT with lattice vectors frozen, which yielded geometric parameters (bond lengths, etc.) in fair agreement with the experimental ones (ESI).

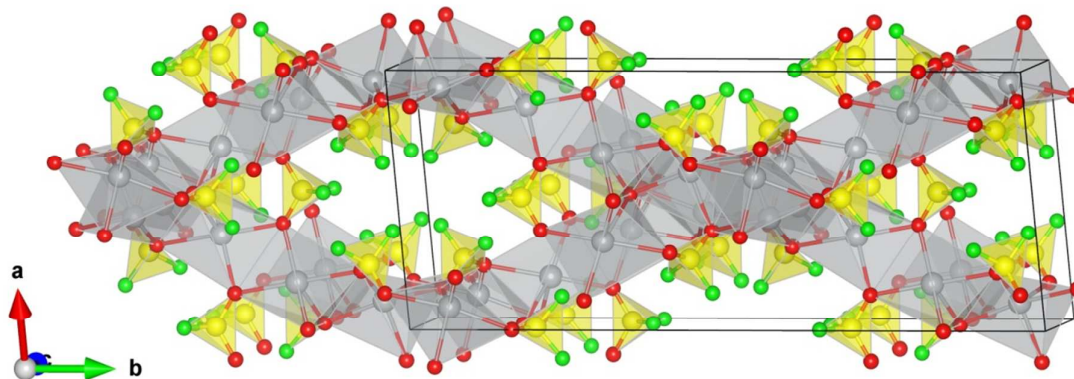
Both difluorophosphates adopt very complex crystal structures. **1** crystallizes³⁵ in the $C2/c$ cell with $Z=16$ (Fig. 1). There are 2 independent Ag^{I} cations and three independent PO_2F_2^- anions in the unit cell with two P atoms occupying special position (on the 2-fold axis). Both Ag^{I} cations are coordinated by 5 oxygen atoms in the form of a square pyramid. Ag-O bond distances are in the range from 2.30 \AA to 2.74 \AA . Due to low coordination number (6 or even 8 would be more suitable for Ag^{I} with oxo ligands) and the presence of at least one long Ag-O bond ($> 2.59 \text{ \AA}$), the remaining Ag-O bonds are relatively short ($2.30\text{--}2.48 \text{ \AA}$). However, the calculated BVS for both Ag atoms is close to 1 (0.978(16) and 0.989(13)), what points at correctness of the refined model and restraints applied. The adjacent $[\text{AgO}_5]$ polygons share one edge and form infinite ribbons $[\text{AgO}_5]_\infty$ which cross at the angle close to 45° (Fig. 1). All PF_2 groups are

terminal, contrary to ionic difluorophosphates like MPO_2F_2 , $\text{M} = \text{K}-\text{Cs}$ ^{19,20}, and fill the space between the ribbons forming infinite 1D tunnels. In each $[\text{AgO}_5]$ polygon one of the O atoms belongs to the neighbouring ribbon.

5 A simplified view of the crystal structure may be obtained if the long Ag-O contacts are neglected; the structure then consists of infinite 1D $[\text{Ag}^{\text{I}}\text{O}_{4/2}]$ chains which are linked into more

complex 3D structures via OPO bridges.

AgPO_2F_2 is formally isoelectronic with AgSO_3F ³⁶ and AgClO_4 .³⁷ However, the complexity of the crystal structure of the former compound ($Z = 8$ in the primitive cell) is enormous as compared to those of its analogues. AgSO_3F crystallizes in primitive monoclinic with $Z = 4$ while disordered AgClO_4 is closed-packed cubic ($Fm\bar{3}m$) with $Z = 1$ in the primitive cell.



15

Fig. 1 View of the crystal structure of AgPO_2F_2 along the 001 direction with $[\text{AgO}_5]$ polygons forming 1D chains intersecting at angle close to 45° .

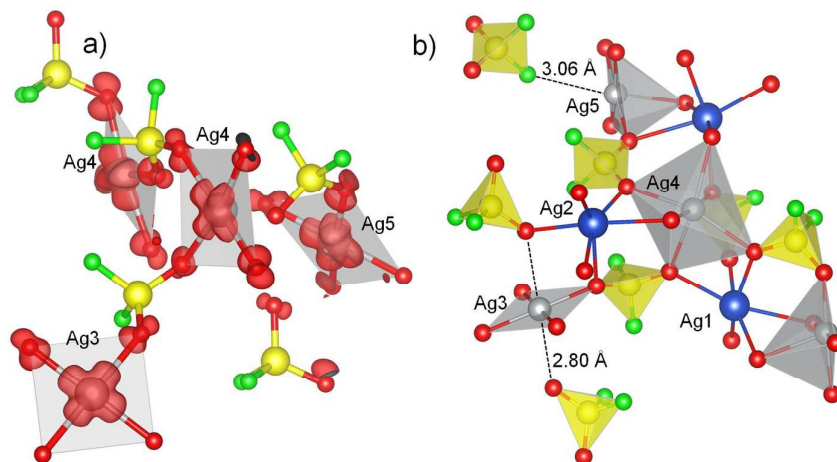
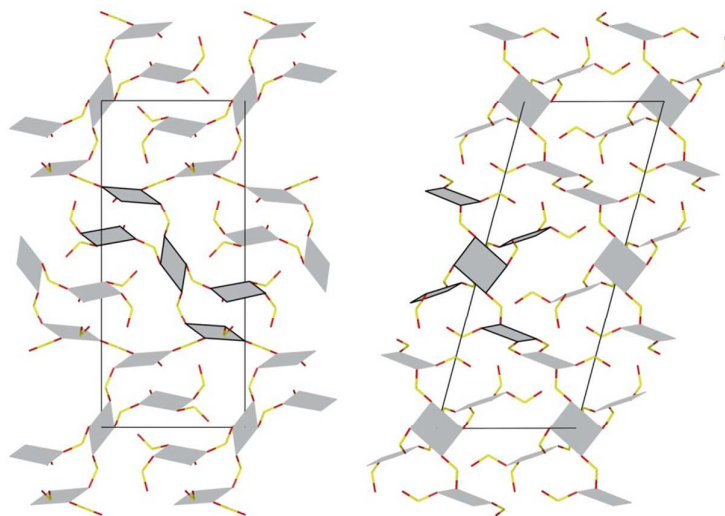


Fig. 2 View of the fragment of the unit cell of $\text{Ag}_9(\text{PO}_2\text{F}_2)_{14}$ presenting (a) spin density visualization and (b) the coordination polyhedra of P(V) (yellow) and Ag(II) (grey) and the first coordination sphere of Ag(I) (blue). Yellow balls: P, red balls: O, green balls: F.



20 **Fig. 3** Two projections of the unit cell of $\text{Ag}_9(\text{PO}_2\text{F}_2)_{14}$ showing the connectivity pattern of the Ag(II)-OPO-Ag(II) bridges and the square planar $[\text{AgO}_4]$ units (longer bonding to apical O in one type of Ag(II) cation has been omitted for sake of simplicity); (a) projection on the bc plane, (b) ac plane. Arbitrarily selected irreducible fragments of the complex polymeric $\text{Ag}(\text{II})_5(\text{PO}_2\text{F}_2)_{14}^+$ sublattice have been emphasized by use of thick black line. Both types of Ag(I) cations as well as F atoms have been omitted for clarity.

Clearly, the increasing number of F atoms which substitute O contributes to the increasing structure complexity. This is because F tends to behave as a terminal ligand at the central main group atom, and it is usually not involved in chemical bonding to metal cations.³⁸ The number of active ligand sites decreasing in the series $\text{ClO}_4^- > \text{SO}_3\text{F}^- > \text{PO}_2\text{F}_2^- > \text{COF}_3^-$ generates coordinatively unsaturated metal sites, enforces ligand-sharing between metal cations, and contributes to structure complexity. It would be interesting to get further insight into this ligand series by preparing $\text{Ag}^{\text{I}}\text{COF}_3$ with only one O atom available for bonding to silver. Regrettably, so far only the three very ionic oxotrifluorocarbonates of heavy alkali metals (K, Rb, Cs) have been prepared and it seems that weaker basicity typical for smaller cations (Ag, Na, Li) and the large lattice energies of MF phases contribute to facile decomposition of MCOF_3 with evolution of COF_2 .

2 ($=\text{Ag}_4^{\text{I}}\text{Ag}_5^{\text{II}}(\text{PO}_2\text{F}_2)_{14}$) crystallizes³⁹ in monoclinic $P2_1/c$ unit cell with $Z = 2$, giving 8 atoms of Ag(I) and 10 atoms of Ag(II) per unit cell. Distinct Ag(I) and Ag(II) sites can be easily distinguished in the structure of **2** (Fig. 2) similarly as for $\text{Ag}_3(\text{SO}_3\text{F})_7$ but contrary to $\text{Ag}_3(\text{SbF}_6)_4$.²⁶ Both of the two independent Ag(I) atoms (Ag1 and Ag2) are coordinated by six O atoms arranged in the form of deformed octahedron. The Ag1-O and Ag2-O distances (2.44–2.76 and 2.41–2.68 Å, for details *cf.* ESI) are reproduced well by DFT calculations. Also the BVS for both atoms is close to 1, which points at correctness of the structure. On the other hand, three various coordination patterns are observed in the case of Ag(II) sites (Fig. 2). The coordination of Ag3 is very similar to that found in AgSO_4 , since there are 4 oxygen atoms forming a square (at 2.080(11) Å and 2.084(11) Å) and the apical O atoms are further apart from silver (2.648(17) Å) than the typical apical O atoms (2.5–2.6 Å) in the $[\text{Ag}^{\text{II}}\text{O}_6]$ octahedra.^{7,9,12} Therefore the coordination of Ag3 can be considered as genuinely square planar. Ag4 is found in an elongated octahedral site with a strong rhombic distortion which leads to a 10% alternation of the equatorial Ag-O bond lengths. (2.250(10) Å/2.252(13) Å *vs.* 2.103(16)/2.099(13) Å). This feature has also been nicely reproduced by DFT calculations (2.26 Å *vs.* 2.15 Å). Finally, Ag5 presents the first example of square pyramidal coordination of Ag(II) in oxo-compound, with only two precedents in the fluoro-compounds *i.e.* $\text{K}_3\text{Ag}_2\text{M}_4\text{F}_{23}$ where $\text{M}=\text{Zr}, \text{Hf}$.⁴⁰ The Ag5-O distances are similar to those found in other oxo-salts. There is one fluorine atom that complements the $[\text{Ag}_5\text{O}_5]$ pyramid to an elongated octahedron, but its distance to Ag(II) of *ca.* 3 Å indicates that there is no significant interaction between the two, what is also supported by IR spectrum as discussed below.

Complexity of the crystal structure of **2** is striking (Fig. 3). With its complex formula, $\text{Ag}_9(\text{PO}_2\text{F}_2)_{14}$ is not far from neither from $\text{Ag}_7(\text{PO}_2\text{F}_2)_{14}$ stoichiometry (*i.e.* metal:ligand 1:2) nor from $\text{Ag}_9(\text{PO}_2\text{F}_2)_{13.5}$ (*i.e.* metal:ligand 2:3). However, the arrangement of cations and anions in this compound is unique and to the best of our knowledge not found in any other inorganic compound. One reaches the same conclusion when analysing the stoichiometry of the anionic $\text{Ag}_5^{\text{II}}(\text{PO}_2\text{F}_2)_4^{4-}$ network. Its composition departs by four anionic ligands from the Ag:P 1:2 stoichiometry (characteristic of a hypothetical neutral $\text{Ag}^{\text{II}}(\text{PO}_2\text{F}_2)_2$) and simultaneously it is one anionic ligand short of the 1:3 stoichiometry (for hypothetical $\text{M}^{\text{I}}\text{Ag}^{\text{II}}(\text{PO}_2\text{F}_2)_3$ salts). Indeed, this implies complex connectivity – as observed (Fig. 3).

The connectivity of adjacent $[\text{AgO}_n]$ polygons in **2** is such that they share only one edge. $[\text{Ag}^{\text{II}}\text{O}_n]$ polygons are always separated by $[\text{Ag}^{\text{I}}\text{O}_6]$ octahedra and do not have any common atoms. This is

consistent with other crystal structures of oxoanionic salts of Ag(II), where no oxygen atom bridging two Ag(II) atoms is present. The reason for that may be that such arrangement in the vicinity of two powerfully electron-withdrawing Ag^{II} cations would cause an immediate oxidation of the oxygen dianion. As a result of the bonding pattern of **2**, the Ag(II) paramagnetic centres from the $[\text{Ag}^{\text{II}}\text{O}_n]$ polygons are connected only through -OPO-bridges (Fig. 2). The geometry of the Ag(II)-OO-Ag(II) fragments, which is important for understanding of magnetic properties, is similar to that found in silver (II) fluorosulfate ($\text{Ag}(\text{SO}_3\text{F})_2$), namely one of the AgOO angles is close to 90° while the other is closer to 180° (*cf.* S-Table 1 in ESI). Every PO_2F_2^- anion is bound to at least one Ag(II) atom using exclusively O atoms. Similarly as in $\text{Ag}(\text{SO}_3\text{F})_2$,⁹ $\text{Cu}(\text{PO}_2\text{F}_2)_2$ ²² or AgPO_2F_2 (described above) all F atoms are terminal and they tend to form F-rich van der Waals cavities.

IR spectra

Table 1. Wavenumbers of the observed IR bands for $\text{Ag}_9(\text{PO}_2\text{F}_2)_{14}$ and AgPO_2F_2 as compared to those measured for $\text{Cu}(\text{PO}_2\text{F}_2)_2$.²²

$\text{Ag}_9(\text{PO}_2\text{F}_2)_{14}$	AgPO_2F_2	$\text{Cu}(\text{PO}_2\text{F}_2)_2$	Assignment
1280 m, sh 1272 vw, sh 1251 vs 1230 vs 1217 w, sh 1191 w, sh	1269 m, sh 1233 vs 1217 s	1289 sh 1263 s 1222 m 1212 m	$\nu_{\text{as}} \text{PO}_2$
1155 m 1129 s 1124 w, sh 1120 s 1105 w, sh 1095 s	1146 s 1120 s 1106 w, sh	1167 s 1145 s	$\nu_{\text{s}} \text{PO}_2$
951 m 941 w, sh 930 s	935 s 919 s 910 w, sh	974 s, sh 953 s	$\nu_{\text{as}} \text{PF}_2$
895 w, sh 891 m 880 m 873 m 870 w, sh	872 m 867 s 860 m, sh	904 s	$\nu_{\text{s}} \text{PF}_2$
559 w, sh 547 w, sh 536 m 513 m 492 m 489 w 485 m 480 w, sh	539 w 521 w, sh 509 m 495 m 485 m	547 m, sh 529 m 497 m	δPO_2 δPOF
375 vw, br 353 vw, br	360 w 355 w	375 vw	δPF_2
273 m 247 m 227 w 203 w 164 w 135 w	225 vw 153 m, br 101 w, br		$\nu_{\text{s}} \text{AgO}$, torsion and lattice vibr.

Band descriptions: vs, very strong; s, strong; m, medium; w, weak; vw, very weak; sh, shoulder; br, broad

In the recorded IR spectra (*cf.* ESI) the $\nu(\text{PO})$ and $\nu(\text{PF})$ are found in the regions typical for covalent metal difluorophosphates.¹⁶ However, as compared to other difluorophosphates, the spread of $\nu_{\text{s}}(\text{PO})$ bands in **2** is very large. This can be explained by the presence of O atoms that are bound very strongly to Ag(II) what causes decrease of the frequency of $\nu(\text{PO})$. There are also two O atoms that form only one bond to Ag(I) and one weak (> 2.5 Å) bond to Ag(II) and therefore give rise to the high frequency $\nu(\text{PO})$ bands. Because in **1** there are O atoms binding either strong or weak to the Ag^I cations, the $\nu(\text{PO})$ are also found in

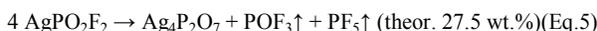
higher and lower frequency regions, but in this case the spread is not as large as for **2**.

The $\nu(\text{PF})$ in **2** are found in the $930\text{--}951\text{ cm}^{-1}$ range for asymmetric and $870\text{--}895\text{ cm}^{-1}$ for symmetric stretches. The extent of their values indicates that F is not a bridging ligand, in agreement with our structural assignments. In the case of Ag(I) salt the $\nu(\text{PF})$ stretches are red shifted as compared to **2**. Analysis of the regions where $\nu(\text{P-F})$ are observed in various metal difluorophosphates¹⁶ reveals a clear tendency, that the position of these bands is dependent on the Lewis acidity of the cation. The higher the acidity, the higher the stretching P-F frequencies. This observation matches the expected trend, since Ag(I) is a moderate Lewis acid, Ag(II) is more Lewis acidic, but Cu(II) is the strongest Lewis acid of the three (and indeed, $\nu(\text{PF})$ bands from Cu(PO_2F_2)₂ are at higher frequencies than for **2**). The positions of bending modes are similar as compared to those for other TM metal difluorophosphates.¹⁶

There are absorption bands in the low frequency region typical of lattice vibrations (around 160 cm^{-1} and 250 cm^{-1}) for both **1** and **2** – which, as based on the theory-supported assignments for other Ag(I) and Ag(II) oxo- salts – likely originate from the stretches and torsions of the entire $[\text{Ag}(\text{I})\text{O}_n]$ and $[\text{Ag}(\text{II})\text{O}_n]$ polygons.^{7,12}

25 Thermal analysis

Thermal stability of each newly prepared chemical compound is of interest and of relevance for its possible applications. The obtained TG and DSC curves for both examined compounds are presented in Fig. 4. **1** starts to lose mass at 160°C in conjunction with melting (broad DSC peak at 180°C). Above this temperature endothermic decomposition accelerates. The process slows down significantly at 269°C when ca. 20% of the initial mass is lost and another endothermic peak is observed. The appearance of this DSC peak seems to be the consequence of rapid change of the decomposition rate of **1** and not any distinct chemical or physical process. Slight mass loss above 269°C may be due to the diffusion of the POF_3 outside the crucible through the pinhole and/or slow decomposition of the remnants of **1** in the bulk of the sample associated with slow diffusion of POF_3 through the bulk. The overall mass drop by ca. 24% corresponds well with those expected for the two alternative decomposition reactions:



A significant heat effect above 300°C , namely an endothermic phase transition at 346°C , which is typical of $\text{Ag}_4\text{P}_2\text{O}_7$,^{41,42} points at the presence of the diphosphate in the sample. A mixture of $\text{Ag}_2\text{PO}_3\text{F}$ and $\text{Ag}_4\text{P}_2\text{O}_7$ (as seen from XRD) usually results from thermal decomposition of AgPO_2F_2 .⁴¹

As judged from the TG curve, thermal decomposition of **2** commences at 120°C , but the noticeable thermal effect appears only above 155°C .⁴³ The process is exothermic and the only gaseous products detected by mass spectrometry are O_2 and POF_3 . This suggests that a redox reaction is a stability-limiting factor for the derivative of Ag^{II} , similarly as for other Ag^{II} oxo-compounds. Above 160°C there is a strong endothermic peak from melting of **1** overlapped with the decomposition of the Ag(I/II) salt causing the complex shape of the DSC curve. There is also an additional smaller endothermic peak at 196°C of unknown origin. At that temperature the mass loss corresponds to 17%. The post-reaction XRD and IR analysis of **2** decomposed on a heating plate at 180°C (until its full decolouration) proves

that at this stage **1** is the only crystalline product of

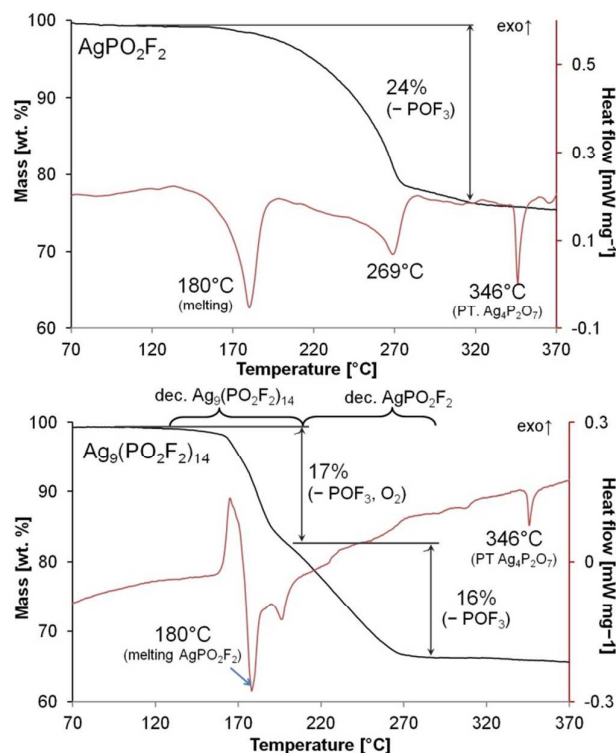
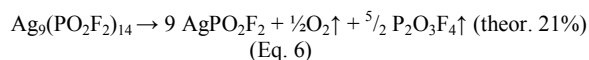


Fig. 4 TGA and DSC curves for thermal decomposition of AgPO_2F_2 (top) and $\text{Ag}_9(\text{PO}_2\text{F}_2)_{14}$ (bottom). PT denotes “phase transition”.

decomposition. These observations suggest the following reaction equation:



There are certain discrepancies between the observed and theoretical mass loss at this stage, as well as chemical identity of the gases evolved (POF_3 vs. $\text{P}_2\text{O}_3\text{F}_4$).⁴⁴ These indicate that, as seen previously for **1**, the course of the thermal decomposition of **2** is more complex than that suggested by a single chemical equation (Eq. 6).

Above 200°C the sample behaves similarly to **1**, although the decomposition rate is rather constant with temperature and consistently the DSC curve shows only a very broad smeared signal. There is also a small endothermic peak around 308°C , which points at presence of small amounts of $\text{Ag}_2\text{PO}_3\text{F}$, as well as the endothermic peak at 346°C , which again points at the presence of $\text{Ag}_4\text{P}_2\text{O}_7$.

As seen from the data presented above, thermal decomposition of silver difluorophosphates is similar to that observed for silver salts of SO_3F^- anion – which is isoelectronic to PO_2F_2^- . Both Ag(I) salts melt at comparable temperatures (156°C for AgSO_3F ,³⁶ 180°C for AgPO_2F_2). What is more, the molecules evolved upon decomposition, namely SO_2F_2 and POF_3 , are also isoelectronic, while the solid residue is composed mostly from silver(I) salt with an anion containing one F atom less than in the parent compound (*i.e.* SO_4^{2-} and PO_3F^- , respectively). Furthermore, fluorosulfates containing Ag(II) (*i.e.* $\text{Ag}(\text{I})_2\text{Ag}(\text{II})(\text{SO}_3\text{F})_7$ and $\text{Ag}(\text{SO}_3\text{F})_9$) decompose in the $120\text{--}140^\circ\text{C}$ range via redox process and with the formation of the corresponding Ag(I) salts, similarly to **2**. One difference is that fluorosulfates evolve peroxofluoride, $\text{S}_2\text{O}_6\text{F}_2$, while the analogous phosphorus species, $\text{P}_2\text{O}_4\text{F}_4$, is quite unstable and therefore **2**

evolves oxygen (similarly to AgSO_4) and phosphorus oxofluorides instead.

Magnetic measurements

The magnetization vs. temperature plot for ZFC and FC measurements of **2** is presented in Fig. 5. The background signal from the Teflon container was subtracted.

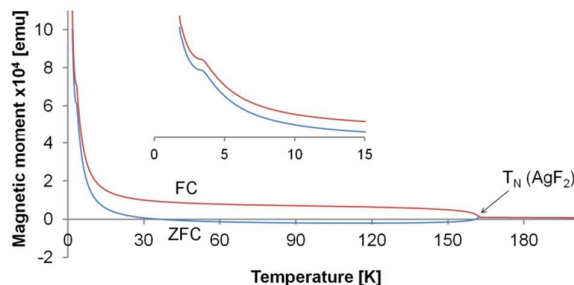


Fig. 5 ZFC (blue, lower) and FC (red, upper) curves for **2**. Inset: magnified low temperature region (2–15 K). T_N denotes Néel temperature for AgF_2 .

The splitting of the ZFC and FC curves below 163 K, as well as the negative signal in the ZFC run are both due to contamination of the sample by traces of the unreacted AgF_2 .⁴⁵ The amount of the contamination estimated from the difference between ZFC and FC curves at 90 K is 3 wt. %. Below 10 K the magnetization rises, and at 3.3 K it shows an inflection point. Due to the unavoidable contamination by AgF_2 detailed analysis of the magnetic moment vs. temperature plots in low (below 20 K) and high (above 170 K) temperature region was not possible. However, based on the crystal structure of the salt, weak ferromagnetic coupling between Ag(II) centres is expected, according to Goodenough-Anderson-Kanamori rules for the bent and close to 90°Ag-O-O-Ag bridges, like in $\text{Ag}(\text{SO}_3\text{F})_2$ where the superexchange pathway is similar.

DFT picture of magnetic properties of $\text{Ag}_9(\text{PO}_2\text{F}_2)_{14}$

We have conducted solid state DFT+U calculations for both **1** and **2**.⁴⁶ The spin-polarized calculations for the ferromagnetic model of **2** localize free spins at $\text{Ag}3$, $\text{Ag}4$ and $\text{Ag}5$ atoms, proving that they truly correspond to divalent silver. The spin density localization (Fig. 2a) shows that the unpaired electrons resides at d_{xy} orbital of Ag(II) , what is in agreement with their elongated coordination. It is also evident that the remaining spin density resides only on the oxygen fragments of the PO_2F_2^- anion. Therefore the magnetic coupling between neighbouring Ag(II) complexes must be realized with the omission of the central atom (here P), as found for other oxo-anionic Ag(II) compounds like AgSO_4 ,⁴ $\text{Ag}(\text{SO}_3\text{F})_2$,⁹ $\text{Ag}_3(\text{SO}_3\text{F})_7$ or $\text{Ag}(\text{SO}_3\text{CF}_3)_2$,¹² where the magnetic coupling is also realized via the $\text{Ag(II)-O}\dots\text{O-Ag(II)}$ bridges.

The band gap calculated for **2** is 2.5 eV indicating that this novel mixed-valence compound of silver should absorb visible light; this is consistent with the observed brown colour of this difluorophosphate derivative.

Comment on $\text{Ag}^{\text{II}}(\text{PO}_2\text{F}_2)_2$, $\text{Cu}^{\text{II}}(\text{PO}_2\text{F}_2)_2$ and $\text{Cu}^{\text{I}}(\text{PO}_2\text{F}_2)$

The rather high thermal stability of $\text{Ag}_9(\text{PO}_2\text{F}_2)_{14}$ indicates that PO_2F_2^- can kinetically withstand the marked oxidizing power of Ag(II) cations. Thus, preparation of quasi-binary $\text{Ag}^{\text{II}}(\text{PO}_2\text{F}_2)_2$ could be thought of, especially that a related $\text{Cu}^{\text{II}}(\text{PO}_2\text{F}_2)_2$ (with a very complicated crystal structure, indeed) has been claimed some 30 years ago.²² While we have clearly failed to reach this

target in our current investigations, we may still think of to-be-prepared $\text{Ag}^{\text{II}}(\text{PO}_2\text{F}_2)_2$ in analogy to its $\text{Cu}^{\text{II}}(\text{PO}_2\text{F}_2)_2$ sibling.

Since **2** corresponds formally to $(\text{AgPO}_2\text{F}_2)_4 \times [\text{Ag}^{\text{II}}(\text{PO}_2\text{F}_2)_2]_5$, a molar volume of hypothetical $\text{Ag}^{\text{II}}(\text{PO}_2\text{F}_2)_2$ may be calculated assuming additivity and using the crystal structure data for **1** and **2**. The value obtained is 158.55 \AA^3 and it is very close to that measured for isoelectronic $\text{Ag}^{\text{II}}(\text{SO}_3\text{F})_2$ ($\sim 161 \text{ \AA}^3$). Interestingly, the theoretical value for $\text{Ag}^{\text{II}}(\text{PO}_2\text{F}_2)_2$ is substantially smaller than the respective value measured for $\text{Cu}^{\text{II}}(\text{PO}_2\text{F}_2)_2$, $\sim 176 \text{ \AA}^3$. This is clearly a discrepancy from the obvious trend that compounds of Ag^{II} have larger molar volumes than those of Cu^{II} (usually by 7–14 \AA^3 per formula unit, Table 2). One possible reason for that may be in structural complexity of difluorophosphates as well as their apparent porosity (due to formation of van der Waals spaces between terminal F atoms).

Table 2. The experimental and estimated (in brackets) volumes per formula unit (in \AA^3) for several related compounds of Cu^{II} and Ag^{II} , as well as Cu^{I} and Ag^{I} , together with the volume differences ($\Delta_{\text{Ag/Cu}}$) between the respective compounds.

Anion	Cu^{II}	Ag^{II}	$\Delta_{\text{Ag/Cu}}$
F^-	34.35	41.40	7.05
SO_4^{2-}	68.17	75.88	7.72
SO_3F^-	(~147-154)	160.97	ND
SO_3CF_3^-	221.4	235.68	14.28
PO_2F_2^-	176.13	(158.55)*	-17.58
Cl^-	64.91	(~72-79)	ND
Anion	Cu^{I}	Ag^{I}	$\Delta_{\text{Ag/Cu}}$
Cl^-	39.81	39.67	-0.14
SO_4^{2-}	89.98	94.12	4.14
SO_3F^-	(~79-83)	83.17	ND
PO_2F_2^-	(~92-96)	95.86	ND

70 ND – not determined; * estimated from crystal structures of **1** and **2**

Using similar comparisons one may derive the expected molar volumes of as yet unknown $\text{Cu}^{\text{II}}(\text{SO}_3\text{F})_2$, $\text{Ag}^{\text{II}}\text{Cl}_2$, $\text{Cu}^{\text{I}}(\text{PO}_2\text{F}_2)$ and $\text{Cu}^{\text{I}}(\text{SO}_3\text{F})$ (Table 2), each constituting an interesting synthetic target *per se*.

Conclusions and prospect

The results presented document progress in structural characterization of metal difluorophosphates with complex crystal structures. They also confirm that extension is possible of rather poorly explored chemistry of the kinetically stable Ag(II) oxygen-bearing compounds, as well as constitute enrichment of the known mixed-valence $\text{Ag}^{\text{II}}/\text{Ag}^{\text{I}}$ systems. The syntheses performed also validate applicability of $\text{P}_2\text{O}_3\text{F}_4$ to obtain PO_2F_2^- salts from corresponding fluorides.

The crystal structures of the both silver salts studied exhibit very complex bonding patterns, with homoleptic ligand environment for both Ag^{I} and Ag^{II} , as well as rare coordination sphere of one particular Ag(II) site (square pyramid [AgO_5]). The mixed-valence $\text{Ag}_9(\text{PO}_2\text{F}_2)_{14}$ is characterized by very weak magnetic coupling with an ordering temperature of *ca.* 5 K. These features can be rationalized on the basis of its crystal structure and using the DFT calculations. Alike other Ag(II) oxoanionic compounds the superexchange is realized via $\text{Ag-O}\dots\text{O-Ag}$ bridges with omission of the central atom in the anion (*i.e.* P).

These results open further interesting research paths. First, careful reexamination is needed of the reaction between AgF_2 and POF_3 , which could lead either to $\text{Ag}^{\text{II}}(\text{PO}_2\text{F}_2)_2$, or to $\text{Ag}^{\text{II}}(\text{OPF}_4)_2$ (both of which are as yet unknown), or to a more complex system. Secondly, synthesis of Ag(II) salt with PO_3F_2^- anion ($=\text{Ag}^{\text{II}}(\text{PO}_3\text{F})$) – which is isoelectronic to sulphate – is also worth to be explored given the poorness of experimental data on monofluorophosphates. Third, the potential of the PO_2F_2^- and

PO_3F^{2-} anions for transmitting very strong antiferromagnetic superexchange in the 180° fashion should be explored (as already documented for isoelectronic SO_3F^- and SO_4^{2-} anions).

Acknowledgements

The project ‘AgCENT: novel unique magnetic and electronic materials based on Ag(II) compounds’ is financed by the Polish National Science Centre (NCN, project UMO-2011/01/B/ST5/06673). Selected measurements were carried out by using the CePT infrastructure financed by the EU European Regional Development Fund within the Operational Programme “Innovative economy” for 2007–2013 (POIG.02.02.00-14-024/08-00). This research was carried out with the support of the “HPC Infrastructure for Grand Challenges of Science and Engineering” Project, co-financed by the European Regional Development Fund under the Innovative Economy Operational Programme within the ICM grant G29-3. We would like also to thank prof. Ingo Krossing for supplying us with HPO_2F_2 used for some part of the syntheses.

Notes and references

²⁰ ^a Laboratory of Novel Functional Materials, Center of New Technologies, University of Warsaw, ul. Żwirki i Wigury 93, 02-089, Warsaw, Poland. Fax: +48 22 5540 801; Tel: +48 22 5540 800; E-mail: malin@cent.uw.edu.pl , dominik.kurzydowski@gmail.com , w.grochala@cent.uw.edu.pl

²⁵ ^b Faculty of Mathematics and Natural Sciences, Cardinal Stefan Wyszyński University in Warsaw, ul. Wóycickiego 1/3, 01-938, Warsaw, Poland

† Electronic Supplementary Information (ESI) available: details of Rietveld refinement and selected results of DFT calculations. See DOI: 10.1039/b000000x/

³⁰ ‡ The crystal structures of **1** and **2** may be obtained Fachinformationszentrum Karlsruhe, 76344 Eggenstein-Leopoldshafen, Germany (e-mail: crysdata@fiz-karlsruhe.de; http://www.fiz-karlsruhe.de/request_for_deposited_data.html) on quoting the CSD numbers: 429712 and 429713, respectively.

- P. Polczyński, R. Jurczakowski, W. Grochala, *Chem. Commun.*, 2013, **49**, 7480.
- W. Grochala, R. G. Egdell, P.P. Edwards, Z. Mazej, B. Žemva, *ChemPhysChem*, 2003, **4**, 997.
- D. Kurzydowski, Z. Mazej, Z. Jagličić, Y. Filinchuk, W. Grochala, *Chem. Commun.*, 2013, **49**, 6262.
- P. J. Malinowski, M. Derzsi, Z. Mazej, Z. Jagličić, B. Gawel, W. Łasocha, W. Grochala, *Angew. Chem. Int. Ed.*, 2010, **49**, 1683.
- P. J. Malinowski, M. Derzsi, A. Budzianowski, P. J. Leszczyński, B. Gawel, Z. Mazej, W. Grochala, *Chem. Eur. J.*, 2011, **17**, 10524.
- W. Grochala, R. Hoffmann, *Angew. Chem. Int. Ed.*, 2001, **40**, 2742.
- T. Michałowski, P. J. Malinowski, M. Derzsi, Z. Mazej, Z. Jagličić, P. J. Leszczyński, W. Grochala, *Eur. J. Inorg. Chem.*, 2011, 2508.
- T. Michałowski, Z. Mazej, A. Budzianowski, Z. Jagličić, P. J. Leszczyński, W. Grochala, *Eur. J. Inorg. Chem.*, 2015, **2**, 324.
- P. J. Malinowski, M. Derzsi, Z. Mazej, Z. Jagličić, P. J. Leszczyński, T. Michałowski, W. Grochala, *Eur. J. Inorg. Chem.*, 2011, 2499.
- F. Aubke, P. C. Leung, *Inorg. Chem.*, 1978, **17**, 1765.
- P. C. Leung, K. C. Lee, F. Aubke, *Can. J. Chem.*, 1979, **57**, 326–329.
- P. J. Malinowski, Z. Mazej, M. Derzsi, Z. Jagličić, J. Szydłowska, T. Gilewski, W. Grochala, *CrystEngComm*, 2011, **13**, 6871.
- M. Eisenberg, D. D. DesMarteau, *Inorg. Chem.*, 1972, **11**, 1901.
- K. Matsumoto, R. Hagiwara, *Inorg. Chem.*, 2009, **48**, 7380.
- C. Schulz, PhD thesis, Albert Ludwig University of Freiburg, Freiburg im Breisgau 2014.
- T. H. Tan, Ph. D. Thesis, The University of British Columbia, 1970.
- K. O. Christie, R. Gnan, R. I. Wegner, W. W. Wilson, *Eur. J. Solid State Inorg. Chem.*, 1996, **33**, 865–877.
- J. Weidlein, *Z. Anorg. Allg. Chem.*, 1968, **358**, 13–20.
- R. W. Harrison, R. C. Thompson, J. Trotter, *J. Chem. Soc. A*, 1966, 1775.

- J. Trotter, S. H. Whitlow, *J. Chem. Soc. A*, 1967, 1383.
- R. W. Harrison, J. Trotter, *J. Chem. Soc. A*, 1969, 1783.
- M. J. Begley, M. F. A. Dove, R. C. Hibbert, N. Logan, M. Nunn, D. B. Sowerby, *J. Chem. Soc. Dalton Trans.*, 1985, 2433.
- S. Schneider, A. Vij, J. A. Sheehy, F. S. Tham, T. Schroer, K. O. Christe, *Z. Anorg. Allg. Chem.*, 2001, **627**, 631.
- Q.-M. Wang, H. K. Lee, T. C. W. Mak, *New. J. Chem.*, 2002, **26**, 513.
- Q.-M. Wang, T. C. W. Mak, *Chem. Commun.*, 2001, 807.
- Z. Mazej, T. Michałowski, E. A. Goreschnik, Z. Jagličić, I. Arčon, J. Szydłowska, W. Grochala, *Dalton Trans.*, 2015, **44**, 10957.
- E. A. Robinson, *Can. J. Chem.*, 1962, **40**, 1725.
- P. A. Bernstein, F. A. Hohorst, M. Eisenberg, D. D. DesMarteau, *Inorg. Chem.*, 1971, **10**, 1549.
- A. I. Liechtenstein, J. Zaanen, *Phys. Rev. B*, 1995, **52**, R5467
- J. P. Perdew, K. Burke, M. Ernzerhof, *Phys. Rev. Lett.*, 1996, **77**, 3865.
- P. E. Blöchl, *Phys. Rev. B*, 1994, **50**, 17953; G. Kresse, D. Joubert *Phys. Rev. B*, 1999, **59**, 1758.
- G. Kresse, J. Furthmüller, *Comp. Mater. Sci.*, 1996, **6**, 15; G. Kresse, J. Furthmüller, *Phys. Rev. B*, 1996, **54**, 11169; G. Kresse, J. Hafner, *Phys. Rev. B*, 1994, **49**, 14251; G. Kresse, J. Hafner, *Phys. Rev. B*, 1993, **47**, 558.
- G. Kresse, D. Joubert, *Phys. Rev. B*, 1999, **59**, 1758.
- K. Momma, F. Izumi, *J. Appl. Crystallogr.*, 2008, **41**, 653.
- Crystal structure data for **1**. AgPO_2F_2 , $M = 208.8$, monoclinic $C2/c$ (no. 15), $a = 11.2617(2)$, $b = 24.2783(5)$, $c = 6.19409(9)$ Å, $\beta = 115.0842(14)^\circ$, $V = 1533.83(5)$ Å³, $Z = 16$, $T = 293$ K, $\rho = 3.6163$, 2θ range: $7\text{--}120^\circ$, step size: 0.013° , 716 reflections measured, $R_p = 14.39\%$, $R_w = 9.47\%$ (R factors defined as in GSAS), $R_B = 6.80\%$.
- W. Grochala, M. K. Cyrański, M. Derzsi, T. Michałowski, P. J. Malinowski, Z. Mazej, D. Kurzydowski, W. Koźmiński, A. Budzianowski, P. J. Leszczyński, *Dalton Trans.*, 2012, **41**, 2034.
- W. Ludwig, R. Warchow, H. J. Berthold, *Z. Kristall.*, 1986, **175**, 283.
- Quite ionic compounds such as certain polymorphic forms of MSO_3F and MCOF_3 ($M = \text{K-Cs}$) constitute exceptions. F does serve as a ligand to alkali cation in these compounds.
- Crystal structure data for **2**. $\text{Ag}_9\text{P}_{14}\text{O}_{28}\text{F}_{28}$, $M = 2384.4$, monoclinic $P2_1/c$ (no. 14), $a = 9.9060(5)$, $b = 10.1870(4)$, $c = 24.1460(10)$ Å, $\beta = 105.1121(18)^\circ$, $V = 2352.37(18)$ Å³, $Z = 2$, $T = 293$ K, $\rho = 3.3652$, 2θ range: $6\text{--}90^\circ$, step size: 0.013° , 1211 reflections measured, $R_p = 15.34\%$, $R_w = 11.87\%$ (R factors defined as in GSAS), $R_B = 7.04\%$.
- D. Koller, B. G. Müller, *Z. Anorg. Allg. Chem.*, 2000, **626**, 1429.
- M. Weil, M. Puchberger, E. Fuglein, E. J. Baran, J. Vannahme, H. J. Jakobsen, J. Skibsted, *Inorg. Chem.*, 2007, **46**, 801–808. It has to be noted that the decomposition product depends on the container in which the sample was decomposed. Thermal decomposition of **1** placed on a hot (300°C) PTFE plate yields a mixture of $\text{Ag}_2\text{PO}_3\text{F}$ and $\text{Ag}_3\text{P}_2\text{O}_7$, as based on XRPD and IR data. However, from TG and DSC curves it is clear that $\text{Ag}_3\text{PO}_3\text{F}$ is not present in the sample heated inside the thermogravimetric analyzer at 300°C , since that would be marked by an endothermic phase transition at 308°C and decomposition above 325°C . The reason for this difference is unclear, but it may be due to secondary reactions between the sample (**1** or its decomposition products) and the evolved POF_3 .
- Thermal decomposition of $\text{Ag}_2\text{PO}_3\text{F}$ is known to yield $\text{Ag}_4\text{P}_2\text{O}_7$.
- The evolved gases are observed by MS above 140°C .
- From the analogy to decomposition of $\text{Ag}(\text{SO}_3\text{F})_2$, where $\text{S}_2\text{O}_6\text{F}_2$ is evolved one could expect that elusive $(\text{PO}_2\text{F}_2)_2$ will evolve. However, the presence of oxygen points at instability of $(\text{PO}_2\text{F}_2)_2$ which could then decompose to $\text{P}_2\text{O}_3\text{F}_4$ and O_2 . On the other hand, $\text{P}_2\text{O}_3\text{F}_4$ could be in equilibrium with POF_3 and PO_2F at elevated temperatures. The mismatch may also originate from secondary reactions of $\text{P}_2\text{O}_3\text{F}_4$ with the Al_2O_3 crucible, stainless steel oven, or SiO_2 capillary which leads to the mass spectrometer. The last but not least, a few parallel decomposition routes might be simultaneously active, also resulting in the amorphous residue which is not detected by XRPD analysis.
- Due to the small and negative remnant magnetic field present during the nominally zero-field cooling AgF_2 spins are frozen in the opposite direction with respect to the field that is switched on during measurement. As a consequence a negative signal is observed up to

the magnetic ordering temperature of AgF_2 (equal to 163 K: P. Fisher, G. Roullet, D. Schwarzenbach, *J. Phys. Chem. Solids*, 1971, **32**, 1641).

- 46 The resulting geometries are consistent with the experimental results. The length of P-F and P-O bonds is overestimated by ca. 3%, what is typical for DFT calculations with most GGA functionals such as PBE used here. The coordination spheres of all silver atoms are also reproduced well. In particular the square pyramidal coordination of Ag5 and rhombic distorted octahedral coordination of Ag4 are confirmed.